# Milling Diagnosis Using Machine Learning Techniques Toward Industry 4.0

Lorraine Codjo, Mohamed Jaafar, Hamid Makich, Dominique Knittel, Mohammed Nouari

# Milling diagnosis using machine learning techniques toward Industry 4.0

**Lorraine Codjo**[1,2], **Mohamed Jaafar**[1], **Hamid Makich**[1],
**Dominique Knittel**[1,2], **Mohammed Nouari**[1]
[1]LEM3, GIP-InSIC, 27 rue d'Hellieule, 88100 Saint Dié des Vosges, France
[2]Faculty of Physics and Engineering, 3 rue de l'Université, 67000 Strasbourg, France

Corresponding author: knittel@unistra.fr

## Abstract

Smart diagnosis of the milling in an industrial environment is a difficult task. In this work, the diagnosis using machine learning techniques has been developed and implemented for composite sandwich structures based on honeycomb core. The goal is to qualify the resulting surface flatness. Different algorithms have been implemented and compared. The time domain and frequency domain features are calculated from the measured milling forces. The experimental results have shown that a good milling diagnosis can be obtained with a Linear Support Vector Machine (SVM) algorithm: good accuracy and short training time.

## 1 Introduction

The Industry 4.0 framework needs new intelligent approaches. Thus, the manufacturing industries more and more pay close attention to artificial intelligence (AI). For example, smart monitoring and diagnosis, real time evaluation and optimization of the whole production and raw materials management can be improved by using machine learning and big data tools [1]. An accurate milling process implies a high quality of the obtained material surface (roughness, flatness) [2]. With the involvement of AI-based algorithms, milling process is expected to be more accurate during complex operations.

T. Mikołajczyk *et al*. developed an Artificial Neuronal Network (ANN) for tool-life prediction in machining with a high level of accuracy, especially in the range of high wear levels, which meets the industrial requirements [3]. The particularity of their work was the combination of a multilayers ANN model with image processing in order to reduce the potential error.
D. Pimenov *et al*. evaluated and predicted the surface's roughness through artificial intelligence algorithms (random forest, standard Multilayer perceptron) [4]: in their investigation the obtained performance depends on the parameters contained in the dataset.
M. Correa *et al*. compared the performances of Bayesian networks (BN) and artificial neural networks for quality detection in a machining process [5]. Even ANN models are often used to predict surface quality in machining processes, they preferred BNs for their significant representation capability and for the fast model building.

In this work, a smart milling diagnosis has been developed for composite sandwich structures based on honeycomb core. The use of such material has grown considerably in recent years, especially in the aeronautic, aerospace, sporting and automotive industries. Recent development projects for Airbus A380 or Boeing 787 confirm the increased use of the honeycomb material. But the precise milling of such material presents many difficulties.

The objective of this work is to develop an industrial surface quality diagnosis for the milling of honey-comb material, by using supervised machine learning methods. Cutting forces are online measured in order to predict the resulting surface flatness.
However, the literature's review does not exhibit deep studies related to the monitoring and the diagnosis of honey-comb core machining in order to ensure flawless surface.

## 2 Experiment description

### 2.1. Workpiece material

The workpiece material studied in this investigation is Nomex® honeycomb cores with thin cell walls. It is produced from aramid fiber dipped in phenolic resin (Fig. 1). The honeycomb cores consist of continuous corrugated ribbons of thin foil bonded together in the longitudinal direction. The aim of such a process is to create a structure allowing lightness and stiffness together thanks to the hexagonal geometry of formed cells. Figure 1 illustrates the geometric characteristics of the honeycomb core.

The use of honeycomb material in sandwich composite is limited by the fragility of each wall of the honeycomb, which influences the quality of obtained surfaces after machining [7, 8, 9].
The Nomex® honeycomb machining presents several defects related to its composite nature (uncut fiber, tearing of the walls), the cutting conditions and to the alveolar geometry of the structure which causes vibration on the different components of the cutting effort [10].

Honeycomb designation: **A10-72-5OX**

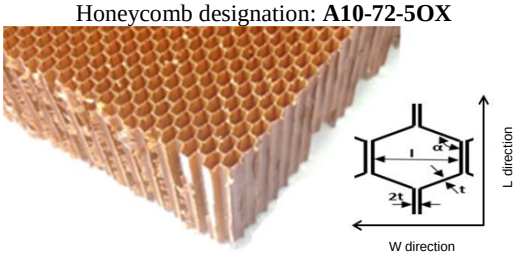


| Density [kg/m3] | Cell size l [mm] | Wall size t [mm] | Angle α [°] |
|---|---|---|---|
| 72 | 5 | 0.08 | 100 |

Figure 1. *Nomex*® honeycomb cores and the main geometrical characteristics.

It is clear that the use of ordinary cutting tools and also the mechanical and geometrical characteristics of honeycomb cores will have a crucial effect on machinability and on the quality of the resulting surface [11].

### 2.2. Cutting tool and experimental environment

For our study, the used milling cutter is provided from our industry partner the EVATEC Tools Company. In fact, ordinary cutting tools for machining honey-comb core produce generally tearing of fibers and delamination of cell structures. Subsequently, these cause a reduction of bond strength between the skin and the honey-comb core, and thus a weaker joint for composite sandwich structures. As shown in figure 2, the EVATEC tool used is a combined specific tool with two parts designed to surfacing/dressing machining operation [12]. The first part is a cutter body made of high speed steel with 16 mm in diameter and having ten helix with chip breaker. This tool part is designated by hogger. The second part is a circular cutting blade made of tungsten carbide with a diameter of 18.3 mm and having a rake angle of 22° and a flank angle of 2.5°. These two parts are mechanically linked to each other with a clamping screw.

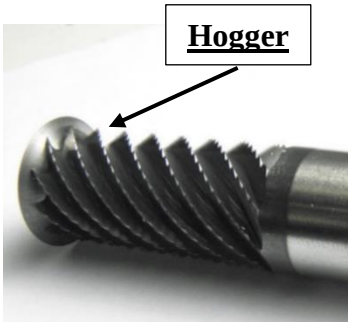


Figure 2. Milling cutter used for Nomex® honeycomb core ‘‘CZ10’’.

Figure 3 shows the forces acquisition setup. During the measurements, the x-axis of the dynamometer is aligned with the feed direction of the milling machine and the longitudinal direction of the workpiece (parallel to core ribbons and the direction of honeycomb double wall). The 3 orthogonal components of machining force (Fx, Fy and Fz) were measured according to figure 3 using the Kistler table [12].

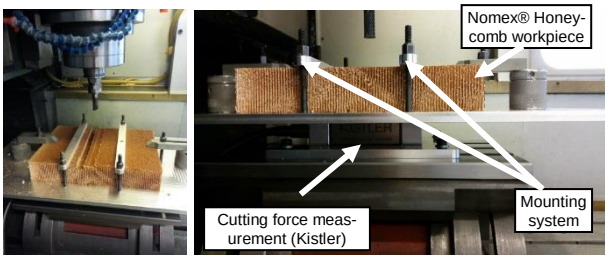


Figure 3. Experimental test setup

| *Realmeca RV8 SP* | |
|---|---|
| *Spindle speed max* | *24 000 rpm* |
| *Feed rate max* | *20 m/min* |
| *Power spindle motor* | *30 kW* |
| *Resolution* | *0.5 µm* |
| *Course X* | *800 mm* |
| *Course Y* | *600 mm* |
| *Course Z* | *450 mm* |

Table 1. Machining center *Realmeca*® RV8 specifications

### 2.3. Milling experiments

All experimental milling tests illustrated in this paper were carried out on a three-axis vertical machining center Realmeca® RV-8. For assessing the performance of the machining process of Nomex® honeycomb core we monitored and measured the cutting forces generated during cutting, by using Kistler dynamometer model 9129AA. The Kistler table is mounted below the Nomex sample in order to measure the three components of the machining force as shown in figure 3.

The milling experiment conditions are summarized in table 2. Four different speeds (high and low speeds) and four feed values were selected.

| Spindle speed (rpm) | 2 000 | 10 000 | 15 000 | 23 000 |
|---|---|---|---|---|
| Feed rate (mm/min) | 150 | 1 000 | 1 500 | 3 000 |

Table 2. Milling experiment conditions.

### 2.4. Measured signals

Figure 4 shows the milling forces measured for honeycomb at 2000 rpm spindle speed and 3000 mm/min feed rate. Cutting forces are in the order of a few Newtons, they do not exceed 60 Newtons. Generally, the force in vertical direction (Fz) is quite small, thus, it is advised that to keeping vertical forces small in milling composite due to the delamination issue. In our case, the vertical cutting force component is greater than other forces components which can be attributed to the mechanical properties of the honeycomb structure where the honeycomb structure is characterized by a better out-of-plane compression behavior than its tensile and shear strength. The evolution of cutting forces shows significant oscillations, these oscillations are caused by vacuum in the cells of the honeycomb and the angle between the cutting direction and the honeycomb cell wall direction.

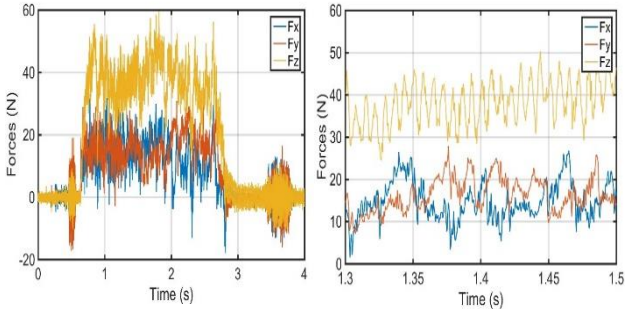


Figure 4. Milling force measurements for 2000 rpm spindle speed and 3000 mm/min feed rate: (a) during all process; (b) during 0.2s (zoom)

Figure 5 shows the evolution of the surface quality (flatness) for various combinations of cutting conditions (spindle speed and feed rate). The defect of shape is higher for low speeds. Thus, for high feed rates that exceed the 1500 mm/min, the unevenness exceeds 500 µm which characterizes the severe tearing of the honeycomb walls.

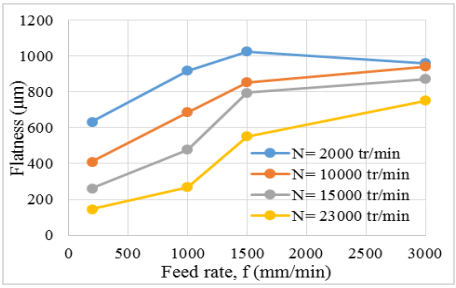


Figure 5. Effect of cutting parameters on surface flatness.

Given the low level of cutting forces, the quality of the obtained machined surface allows to establish criteria for determining the machinability of the honeycomb structures. The appearance of the uncut fibers is a machining defect specific to the composite material which depends on the type of the fibers and their orientation. The tearing of Nomex® paper, linked to the cellular appearance of the honeycomb structure, occurs under the effect of shear loading [12, 13].

# 3 Milling diagnosis using machine learning techniques

There are many approaches in machine learning. The two principals are [15] :
- Unsupervised approaches : based only on input data (unlabeled data) ; the goal is to find a natural grouping or structuring in the data set in order to reduce the number of observations ;
- Supervised approaches: based on input and output data (labels).

Supervised learning algorithms (with labeled data) can split in two categories [15] :
- Classification models which partition observations in categorical groups (leads to a predictive model for discrete responses).
- Regression models which describe the relationship between outputs and variables through a mathematical function (leads to a predictive model for continuous responses).

Our work focused on supervised learning for the classification of data according to predefined specific classes.

## 3.1 Features calculation

The features are calculated in time domain and frequency domain from the raw signal represented on figure 4, in steady state behavior (transient zones, i.e. the time zone when the cutting tool enters into the honeycomb core and the zone when it exits, are not taken into account). The milling force plotted in figure 4 is the vertical force (Fz) of a given milling. That force is negative due to the fact that the z-axis direction of the dynamometer has been oriented downwards

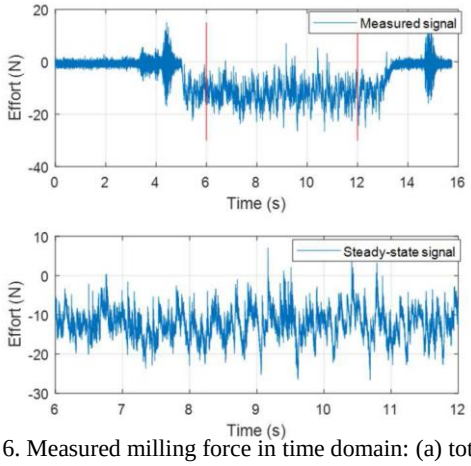


Figure 6. Measured milling force in time domain: (a) total data plot, (b) signal during steady-state phase

After a first data processing (filtering), firstly many features are calculated in time domain for the measured milling force signal called hereafter *x*(t).

The calculated time domain features are:

- maximum of x(t) (1)

- minimum of *x*(t) (2)

- difference between the maximum of x(t) and the minimum of x(t) : amplitude range (3)

- median value of *x*(t) (4)

- Maximum of the absolute value of the signal :

$$m_{AS} = max(|x_k|) \quad (5)$$

- Interquartile range :

$$IQR = Q_3 - Q_1 \quad (6)$$

where $Q_3$ and $Q_1$ represents respectively the upper and lower quartile.

- Inter decile range :

$$IDR = D_{90} - D_{10} \quad (7)$$

where $D_{90}$ and $D_{10}$ means respectively the 90$^{th}$ ant the 10$^{th}$ decile. Both Inter quartile and Inter decile range are a measure of statistical dispersion of the values in a set of data.

- Average value of the signal :

$$mean(x) = \frac{1}{N}\sum_{k=1}^{N} x_k \quad (8)$$

- Average value of the absolute value of the signal :

$$MAS = \frac{1}{N}\sum_{k=1}^{N} |x_k| \quad (9)$$

- Average value of the absolute value of the derivative signal :

$$MAD = \frac{1}{N-1}\sum_{k=1}^{N-1} |\frac{dx_k}{dt}| \quad (10)$$

- Variance :

$$Var = \frac{1}{N}\sum_{k=1}^{N} \big(x_k - mean(x)\big) \quad (11)$$

- Energy of the signal :

$$E(x) = \sum_{k=1}^{N} {x_k}^2 \quad (12)$$

- Energy of the centered signal :

$$E_c = \sum_{k=1}^{N} \big(x_k - mean(x)\big)^2 \quad (13)$$

- Energy of the derivative signal :

$$E_d = \sum_{k=1}^{N-1} \left(\frac{dx_k}{dt}\right)^2 \quad (14)$$

- Skewness :

$$S = \frac{E\big(x - mean(x)\big)^3}{Var^{3/2}} \quad (15)$$

- Kurtosis :

$$K = \frac{E\big(x - mean(x)\big)^4}{Var^2} \quad (16)$$

- Moment order i (i = 5 : 10) :

$$m_i = \frac{E\big(x - mean(x)\big)^i}{Var^{i/2}} \quad (17)$$

- Shannon entropy :

$$E_S(x) = -\sum_{k=1}^{N} {x_k}^2 * \log_2({x_k}^2) \quad (18)$$

- Signal rate :

$$\tau = \frac{max(x_{k=1:N}) - min(x_{k=1:N})}{mean(x)} \quad (19)$$

Secondly 19 features are calculated in frequency domain in a similar way for the measured milling force signal. Therefore, the Fast Fourier transform (FFT) of the signal x(t) has been calculated :

$$Y(k) = \sum_{i=1}^{N} x_i e^{-j2\pi k\frac{i}{N}}, (k = 1, \dots, N) \quad (20)$$

where N is the number of samples of the signal x(t).

The frequency domain features are calculated for the Y(f) signal. For example the Fast Fourier transform (FFT) plot is given on figure 7.

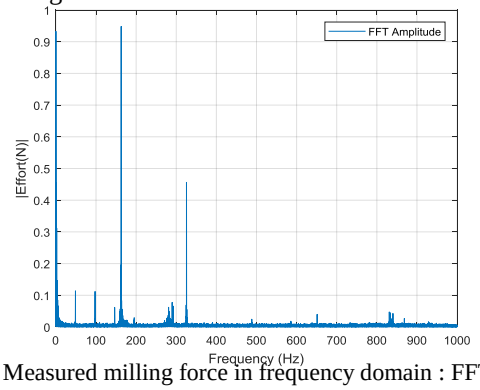

Figure 7. Measured milling force in frequency domain : FFT plot.

All the calculated features (in time and frequency domains) have been normalized and stored in a table whose lines and columns respectively represent the physical experiments and the associated feature values.

**Normalization**

The resulting features being of different units and scale, it is necessary to normalize them in order to avoid meaningless and redundant information. The chosen normalization is given by the equation 21 [14] :

$$feature_{norm} = \frac{feature - \mu(feature)}{\sigma(feature)} \quad (21)$$

where $\mu$ and $\sigma$ represent respectively the mean value and the standard deviation of each column of feature type.
This normalization leads to :

$$\begin{cases} \mu(feature_{norm}) = 0 \\ \sigma(feature_{norm}) = 1 \end{cases}$$

The normalized features are dimensionless and can thus be compared. The normalized feature table contains 39 features and 3 input parameters for each experiment: the rotation speed, the cutting speed and the depth of cut (i.e. the quantity of material the tool will take during milling).

**Feature reduction**

It is necessary to reduce the number of features in order to avoid overfitting on one hand and on the other hand to reduce the online computing time of the features. That dimensional reduction was made, by using the Principal Component Analysis (PCA) [19]. PCA can be seen as a data pre-processing method which leads to a weighted reduced matrix Z where each principal component $Z^n$ (column of Z) is a linear combination of all the original variables ($X^p$) [19]:

$$Z^n = \alpha^{1n}X^1 + \alpha^{2n}X^2 + \cdots + \alpha^{pn}X^p \quad (22)$$

Based on a pareto plot of the principal component variances (fig. 8), the reduced dataset can be obtained by keep-

ing only the m-first principal components which allow to reach a variance percentage of 99%. In our experimental case, m=9. So only the nine first principal components are kept.

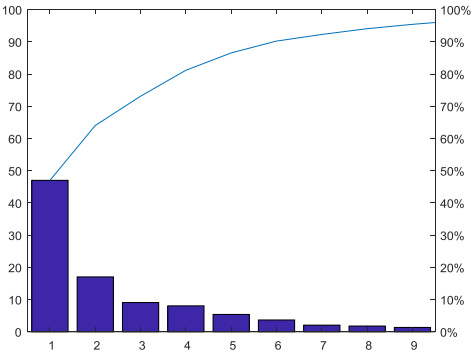


Figure 8. Pareto plot of the variance percentage.

### 3.2 Labeled data

From the evaluation of the effect of the cutting parameters on surface flatness results, we defined two classes of surface quality applied to the output data of each observation (see table 3) :

| Label | Flatness (µm) | Qualitative value |
|---|---|---|
| 'A' | 0 – 600 | Best surface quality |
| 'B' | 600 – … | Worst surface quality |

Table 3. Label table for the experimental observations.

As shown in table 3, we have two labels, called classes. Class 'A' corresponds to the positive class, Class 'B' corresponding to the negative class. News data will be predicted using the rules below:

- If prediction probability result ≥ 0.5 : class A
- If prediction probability result < 0.5 : class B

**Training and validation set**

The data were reduced in a training subset (used to train the classification algorithm) and a test subset (for the validation). For selecting the observations in each data subset, a random logical selection was made. The table below resumes the partition of the data used in each classification algorithm.

| Dataset | Percentage | Class A | Class B | TOTAL |
|---|---|---|---|---|
| Training | 70% | 15 | 20 | 35 |
| Test (Validation) | 30% | 6 | 8 | 14 |
| TOTAL | 100% | 21 | 28 | 49 |

Table 4. Partition of the data.

### 3.3 Supervised learning

In this work, several classification algorithms have been implemented in the Matlab software environment (with the Matlab Statistics and Machine Learning Toolbox, Version: R2017) :

- k-nearest neighbor (kNN)
- Decision tree (DT)
- Support Vector Machine (SVM)

In order to evaluate how the internal parameters of each algorithm influence their efficiency, several variants of the same algorithm have been implemented (various distances, different kernels, etc.).

The first k-nearest neighbor (KNN) was implemented by keeping the default Euclidean distance. For the same model, a limited number of neighbors (k=2) have been applied. Another training model consisted to weight each observation (the rows of our data set). Moreover the KNN algorithm has been modified by using the Chebychev distance.
The first used decision tree algorithm is a fitted binary classification decision tree. Then tree has been pruned to obtain a pruning tree of level 2.
Two SVM algorithms have been implemented using different kernel functions. The first one is a linear SVM which is the default function for a two-class data set. The second one is the Gaussian SVM algorithm which is a normalized polynomial kernel.

## 4 Obtained results

### 4.1 Results of the trained models

Table 5 shows the accuracy result of each algorithm performed with the complete normalized data set

| Algorithms | Accuracy (in %) |
|---|---|
| KNN | 100% |
| KNN k=2 | 88.6% |
| Weighted KNN k=2 | 83.4% |
| Chebychev KNN k=2 | 100% |
| Tree | 100% |
| Pruned tree | 66.67% |
| Linear SVM | 91.4% |
| Gaussian SVM | 91.4% |

Table 5. Prediction error for the normalized data set.

From table 5 we can observe that the simple decision tree classifier leads to the best trained model for predicting new data. But when that same algorithm was pruned, it lost an accuracy of 32.33%.

| **Algorithms** | **Accuracy** |
|---|---|
| kNN | 99% |
| kNN k=2 | 85% |
| Weighted kNN k=2 | 98.2% |
| Chebychev kNN k=2 | 87.5% |
| Tree | 99.2% |
| Pruned tree | 66.67% |
| Linear SVM | 99.8% |
| Gaussian SVM | 93.8% |

Table 6. Prediction error for the Label table for the n-by-n weighted matrix.

Table 6 shows the accuracy result of each algorithm performed with the reduced normalized data set (obtained from the PCA).
A first conclusion is that for a dimension reduced feature table, the algorithms gave better results. From table 5 (which presents the accuracy result from the weighted reduced data set), it could be noticed that both three algorithms produces high accuracy rate for no-parametric algorithm. Specifically, linear SVM is the most efficient with

the lowest running time and the highest accuracy. It is also noticed that more an algorithm is constrained by parameters, more its performances are reduced. It is the case of the pruned tree for which we limit the expansion: it is difficult for the model to find the best singleton split.

### 4.2 Prediction results for new experiment data

We used some news experimental data set in order to evaluate the performance of the trained model. The goal is to predict online (during milling) the surface quality. Results are presented here for the trained model by using the linear SVM classifier algorithm. Table 7 shows the percentage of true positive rate and false negative rate obtained from the evaluation of the prediction.

| | Predicted class | | |
|---|---|---|---|
| Actual class | A | B | |
| A | TP = 61.5% | FN = 38.5% | 100% |
| B | FP = 0% | TN = 100% | 100% |

(TP: true positive rate; FN: false negative rate; FP: false positive rate; TN: true negative rate)

Table 7. Performance of the prediction using SVM classifier.

The negative class B was the best predicted class. This is simply explained by the fact that it is the most predominant class in the data set.

The linear SVM algorithm loses in performance for data set with large predictors (i.e. large features). However, with the reduced number of of features (9_first principal components), this algorithm has been the most accurate algorithm with the best prediction rate for the lowest training time.

## 5 Conclusion and further works

The milling's quality is qualified by the roughness or the flatness of the resulted surface. In this work, different supervised learning algorithms have been implemented (offline) and compared. Each AI-based model has been applied to a set of features. These features were calculated from measured milling forces.

From the prediction results, SVM algorithm seems to be the most efficient algorithm in this application.

The next step consists to implement an online version (therefore the features have to be calculated online).

## References


[1] Beskri A. et al., "Systèmes de surveillance automatique en usinage: Moyens et méthodes" (translation: Automatic monitoring systems in machining: Ways and methods), French Mechanics Congress 2013.

[2] IFPM-Formation, Usinage: Tournage Fraisage (translation; Machining: Milling Turning), September 2015.

[3] Mikołajczyk T., K. Nowicki, A. Bustillo, D. Yu Pimenov, "Predicting tool life in turning operations using neural networks and image processing", Mechanical Systems and Signal Processing, 104: 503-513, 2018.

[4] Pimenov D. Yu, A. Bustillo, T. Mikolajczyk, "Artificial intelligence for automatic prediction of required surface roughness by monitoring wear on face mill teeth" Journal of Intelligent Manufacturing, 29(5): 1045-1061, 2018.

[5] Correa M., C. Bielza, J. Pamies-Teixeira, "Comparison of Bayesian networks and artificial neural networks for quality detection in a machining process", International journal of Expert Systems with Applications, 36: 7270-7279, 2009.

[6] A.I.H. Committee, ASM Handbook Volume 16: Machining, ASM International, 1989.

[7] J. Kindinger, Lightweight structural cores, ASM Handb. Met. Composites, 21: 2001.

[8] D. Gay, Matériaux composites (translation: Composite materials), Hermes, 2015.

[9] R. Carl, "Three-dimensional honeycomb core machining apparatus and method", US Pat. App. 13/707,670. 1, 2012.

[10] Jaafar M., S. Atlati, H. Makich, M. Nouari, A. Moufki, B. Julliere, "A 3D FE modeling of machining process of Nomex® honeycomb core : influence of the cell structure behaviour and specific tool geometry", Procedia CIRP, 58: 505-510, 2017

[11] Mendoza M.M., K. F. Eman, S. M. Wu, "Development of a new milling cutter for aluminum honeycomb", Int. J. Machine Tool Design Research vol. 23: 81-91, 1983.

[12] Jaafar M., H. Makich, S. Atlati, M. Nouari, B. Julliere, "Etude expérimentale et numérique de l'usinage des structures composites en nid d' abeilles Nomex®", in National French congress : Journées Nationale sur les Composites 2017.

[13] H. Tchoutouo and N. Gandy, "Adhesiveless honeycomb sandwich structure with carbon graphite prepreg for primary structural application: a comparative study to the use of adhesive film" May 2012.

[14] Gopal S. and Kishore K., "Normalization: A Preprocessing stage", CSE & IT department, VSSUT, Burla, India 2015.

[15] Shalev-Shwartz S. and Ben-David S., "Understanding Machine Learning: From Theory to Algorithms", Published by Cambridge University Press, 2014.

[16] Rion J., Y. Leterrier, J.-A. E Manson, "Prediction of the adhesive fillet size for skin to honeycomb core bonding in ultra-light sandwich structures" Compos. Part A, 39: 1547-1555, 2008.

[17] Ompusunggu A. P., B. Kilundu, T. Ooijevaar, S. devos, "Automated bearing fault diagnostics with cost effective vibration sensor", WCEAM/VETOMAC 2017 Conference, Brisbane, Australia

[18] Madhusudana C.K., S. Budati, N. Gangadhar, H. Kumar, S. Narendranath, "Fault diagnosis studies of face milling cutter using machine learning approach", Journal of Low Frequency Noise, Vibration and Active Control, 35(2): 128-138, 2016.

[19] Richardson M., "Principal Component Analysis", course May 2009.

[20] Fu Y., Y. Zhang, H. Qiao, D. Li, H. Zhou, J. Leopold, "Analysis of feature extracting ability for cutting state monitoring using deep belief networks", Procedia CIRP, 31: 29-34, 2015.

[21] Gao C., W. Xue, Y. Ren, Y. Zhou, "Numerical control machine tool fault diagnosis using hybrid stationary subspace analysis and least squares support vector machine with a single sensor", MDPI conference, 7: 346-358, 2017.

[22] Zhang C., X. Yao, J. Zhang, H. Jin, "Tool Condition Monitoring and Remaining Useful Life Prognostic Based on a Wireless Sensor in Dry Milling Operations", Sensors journal, MDPI, 16: 795-815, 2016.